energies

MDPI

Article

Hard Carbon Reprising Porous Morphology Derived from Coconut Sheath for Sodium-Ion Battery

Meenatchi Thenappan, Subadevi Rengapillai * and Sivakumar Marimuthu *

#120, Energy Materials Lab, Department of Physics, Science Block, Alagappa University, Karaikudi 630003, Tamil Nadu, India

* Correspondence: subadevir@alagappauniversity.ac.in or susimsk@yahoo.co.in (S.R.); sivakumarm@alagappauniversity.ac.in or susiva73@yahoo.co.in (S.M.); Tel.: +91-4565-223-306 (S.R.); +91-4565-223-304 (S.M.)

Abstract: Seeking effective energy technology has become a herculean task in today's world. Sodium-ion batteries play a vital role in the present energy tech market due to their entrancing electrochemical properties and this work is a breakthrough for developing sodium-ion batteries. As per recent reports, the preparation of anode materials seems to be very tedious in the realm of sodium-ion batteries. To remedy these issues, this work enlightens the preparation of hard carbon (HC) derived from coconut sheath (CS) by a pyrolysis process with different activating agents (KOH, NaOH, $ZnCl_2$) and employed as an anode material for Sodium-ion batteries (SIBs). The prepared anode material was characterized for its thermal, structural, functional, morphological, and electrochemical properties. Additionally, the surface area and pore diameter of the as-prepared anode material was studied by nitrogen adsorption and desorption isotherm methods. The coconut sheath-derived hard carbon (CSHC) anode material delivered an initial charge capacity of 141 mAh g^{-1}, 153 mAh g^{-1}, and 162 mAh g^{-1} at a 1 C rate with a coulombic efficiency over 98.8%, 99.3%, and 99.5%, even after 100 cycles, respectively.

Keywords: coconut sheath; hard carbon; pyrolysis process; anode material; sodium-ion batteries

check for updates

Citation: Thenappan, M.; Rengapillai, S.; Marimuthu, S. Hard Carbon Reprising Porous Morphology Derived from Coconut Sheath for Sodium-Ion Battery. *Energies* **2022**, *15*, 8086. https://doi.org/10.3390/en15218086

Academic Editor: Andrea Reverberi

Received: 9 October 2022
Accepted: 27 October 2022
Published: 31 October 2022

Publisher's Note: MDPI stays neutral with regard to jurisdictional claims in published maps and institutional affiliations.

Copyright: © 2022 by the authors. Licensee MDPI, Basel, Switzerland. This article is an open access article distributed under the terms and conditions of the Creative Commons Attribution (CC BY) license (https://creativecommons.org/licenses/by/4.0/).

1. Introduction

A large variety of electrode materials for energy storage applications are being established in order to create a sustainable and green technologies, thereby overcoming the environmental and energy crisis. An enhanced electrochemical performance of the electrode significantly depends on the structure, morphology, and size of the particles. The structure and morphology have a significant role in the chassis of anode materials. Typically, hard carbon (HC)-based materials are optimal among all the other anodic materials in sodium batteries as they demonstrate high storage capacity, cycling stability, and fairly low working potential. In general, HC has a disordered and irregular structure in which layered carbon atoms are closely and randomly connected. They are mechanically hard when compared to graphite that cannot be deformed into crystalline graphite by simple heating. HC are environmentally benign, inexpensive, and can be obtained from sustainable bio sources, which signifies a great advantage in terms of cost, commercialization, and large-scale production [1,2]. Generally, graphite is used as a negative electrode for LIBs. Here, due to the crystal structure of graphite, the Na ions will not be able to store and release into the graphite [3,4]. This is due to the ionic radius of Na ions. The atomic size of Na (1.02 Å) is greater than Li (0.69 Å). Hence, it could not intercalate into graphite to form binary graphitic intercalation (b-gic). This is due to the weak chemical bonding with graphitic carbon. The suitable remedy for this complication is to work out the materials with large pore sizes like HC. However, these HCs require greater interlayer separation for free intercalation/deintercalation of Na ions to attain good electrochemical

performance. Additionally, the porous nature of the materials further assists in Na ion storage by reversible ion transfer process through the pores [5].

However, biomass-based hard carbon evinces superior electrochemical properties in sodium-ion batteries. The weak cycling performance and low coulombic efficiency retard the marketable applications of carbon as anode electrode materials for SIBs. To overcome these issues, picking proper biomass precursors of hard carbon should be the most significant aspect. Currently, the lack of fuels and the ecological problems have trained the attention on justifiable and renewable resources for the energy storage system. As a result, the concept of renovating bio-waste into beneficial carbon material is procuring more and more attention. Banana peel, orange peel, lotus petiole, okra by-product, peanut shells, natural wood fibers, or compact wood have rendered acceptable performance while employing Na–ion [6–16]. Two processes are involved in the preparation of hard carbon. First, in an inert atmosphere, the raw bio precursor is Pyrolysed and escorted by chemical or physical activation at a high temperature. Steam and carbon dioxide are the physical activators of the precursors. KOH, NaOH, H_3PO_4, and $ZnCl_2$ are well-known chemical activators. These chemical activating agents have been employed to bring porosity to carbon for copious applications. Among them, KOH, NaOH, and $ZnCl_2$ are the most delectable chemical reagents for the activation process of carbon used in batteries because they yield high carbon, precise pore size distribution, high porosity, and surface area. For many years, the international market lent various coconut sector outputs for sale that included copra, crude coconut oil, and its derivatives. The mass production of coconut is primarily focused on coastal regions and subtropical Asia, which represents 86% of the 12 million hectares embedded in the world [17]. The geological origin of the coconut plant is supposed to be in this part of the world. Coconut can be served as a food product and provides various applications in daily life. CS is a part of the coconut tree that is found in the tip and base of the tender leaves. It has the tendency to protect the leaves from global climatic conditions and micro-organisms. CS is traditionally used for wound healing. Like other parts it also has fibrous and porous nature. This structure also helps to stop bleeding like cotton bandages. This property is due to the joint effect of antimicrobial activity, the growth-promoting factors, and its fibrous structure [18]. It also has high lignin content and is mainly composed of cellulose and hemicelluloses [19].

This work promotes the preparation of hard carbon using chemical activating agents (KOH, NaOH, and $ZnCl_2$) by the traditional or conventional pyrolysis process. Herein, we employ an attractive alternative waste coconut sheath for producing hard carbon to serve as an anode for Na ion batteries. It is a cost-effective, extensively available, and sustainable source of carbon. It reveals better cycling performance by using sodium metal as a cathode electrode. This work explores the effect of coconut sheath combined with a precursor that is truly an abundant waste that will make these electrodes both inexpensive and ecologically friendly.

2. Experimental Procedure

2.1. Synthesis of Coconut Sheath Derived Hard Carbon (CSHC)

The coconut sheath (CS) was dried at 220 °C overnight. Then the dried, crushed, and ground CS samples were initially calcined at 500 °C for 2 h. The chemical activating agents KOH, NaOH, and $ZnCl_2$ were used to activate the above samples. Moreover, raw CS precursor was immersed into activating agents and kept overnight for aging at ambient temperature. After the aging process, the material was dried at 110 °C. The dried CS powder was then pyrolyzed at 900 °C for 2 h at a rate of 5 °C min^{-1} under argon flow. The carbonized CS was then washed with 2 M HCl and deionized water. The obtained sample was again dried at 110 °C overnight in an oven. The final product CSHC was obtained. The schematic representation of the as-prepared sample is presented in Figure 1.

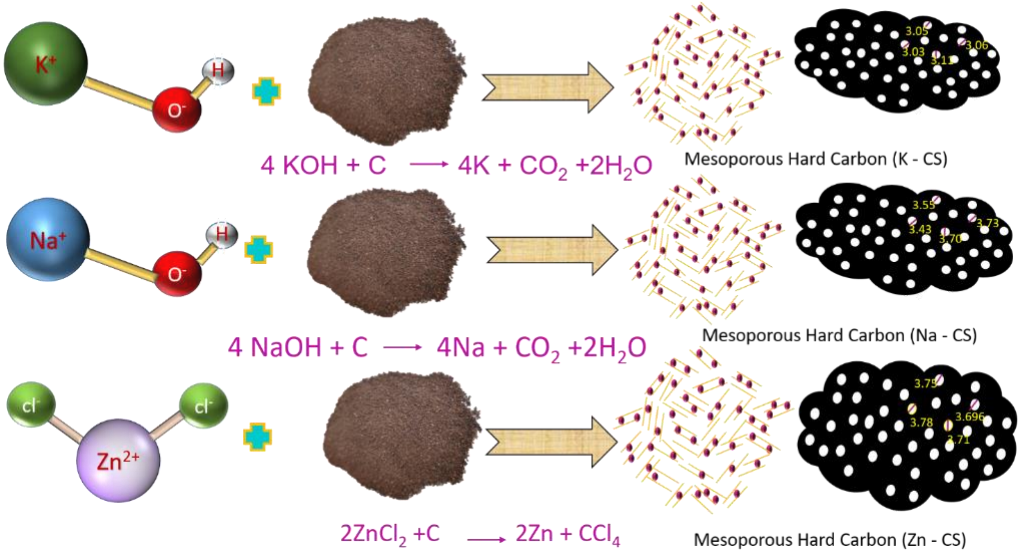


Figure 1. Schematic representation of the synthesized CSHC.

2.2. Structural Characterizations

The thermal stability of the synthesized sample (CS) was evaluated by thermogravimetry (TG) and differential thermal analysis (DTA) (SIINT 6300 TG DTA) between 30–1000 °C with Alumina crucibles under N_2 atmosphere at a heat rate of 20 °C/min. The amorphous nature of the material was examined by powder X-ray diffraction (PAN analytical, X'-pert pro model) analysis with Cu K_α radiation (λ = 1.5406 Å) in the range 2θ = 10–80°. Raman spectroscopy STR RAMAN, SEKI Corporation (Japan) was used to recognize the presence of amorphous disordered carbon phases in the prepared sample. The functional group of the material was analyzed by Fourier transform infrared spectrometer (PerkinElmer) in the range of 400–4000 cm^{-1}. The morphology of the carbon sample was determined by scanning electron microscopy (Quanta FEG 250). Transmission electron microscopy was accomplished to study the surface morphology of the synthesized powder using the JEOL Hi-Resolution Transmission Electron Microscope, Japan. The specific surface area and pore size can be measured by the BET (Brunauer–Emmett–Teller) method (Nova station A).

2.3. Electrochemical Studies

The electrochemical analysis of the synthesized materials (K-CS, Na-CS, Zn-CS) was analyzed using a CR-2032 type coin-cell congregated in an argon (Ar)-filled glove box. The negative anode electrode coated onto the aluminum foil was a combined mixture of 75% active electrode material, 15% Super-P carbon, and 10% polyvinylidene fluoride (PVdF). Sodium metal was used as a positive electrode. 1 M $NaClO_4$ in ethylene carbonate (EC) and diethylene carbonate (DEC) was used as an electrolyte. The cyclic voltammetry (CV), and charge/discharge measurements were examined using a biologic (BCS-815, France) battery tester between 0.01 and 3 V vs. Na/Na^+ cell couple at ambient temperature.

3. Results and Discussion

The as-pyrolyzed coconut sheath hard carbon is named as X–CS, where X indicates the activating agents used (Potassium hydroxide–K, Sodium hydroxide–Na, Zinc chloride-Zn). Owing to perceiving an appropriate anode material for SIB, three various activating agents were used and permitted to react with the material to provide a more porous nature.

Initially, the coconut sheath (CS) was chopped into small pieces and dried in sunlight for three days. Then the precursor was dried at 210 °C to vaporize the water molecules and their residues. Generally, the structure of CS consists of biopolymers and includes high lignin content, hemicellulose, and cellulose. In this context, the hemicellulose and lignin are highly interconnected and amorphous, thus gratifying the emergence of non-graphitic

carbon at reasonable pyrolysis temperature. The CS sample flinches its weight loss from room temperature to final temperature, due to the thermal degradation of the structural components present in the CS sample. Henceforth, in thermal analysis, the decomposition process undergoes three steps in a particular order. Initially, the hemicellulose starts to degrade with the subsequent degradation of cellulose and lignin [16,20]. Here, from 30 to 150 °C, the preliminary loss of mass (~9%) is due to the removal of water molecules. The upcoming losses of weight are primarily because of the degradation of main structural components, including hemicellulose, cellulose, and lignin. The peak ranges between 150 to 350 °C are exothermic, designating a huge weight loss (~6%). The degradation of hemicellulose takes place at 200 to 260 °C. It includes galactose, glucose, mannose, arabinose, and xylase [21]. After the completion of hemicellulose degradation, the cellulose degradation starts at 296 °C. Eventually, the lignin degrades gradually in all ranges of temperature up to 550 °C. Finally, (~17%) of weight loss of the raw coconut sheath precursor takes place. Furthermore, there is no weight loss beyond 550 °C. Hence, the structural degradation and weight loss of the CS precursor were confirmed by TGA analysis and shown in Figure 2. Because of these, lignin plays a significant role in producing porous carbons from biomass through the pyrolysis process. During the pyrolysis process, the biological molecules emit gasses such as CO and CH_4. These organic molecules thus avoid the generation of graphite which has tiny interlayer spacing to facilitate Na ion intercalation. Though, the resultant hard carbons are also extremely defective. Additionally, it can be observed that DTA has the same decomposition profile together with intense exothermic peaks.

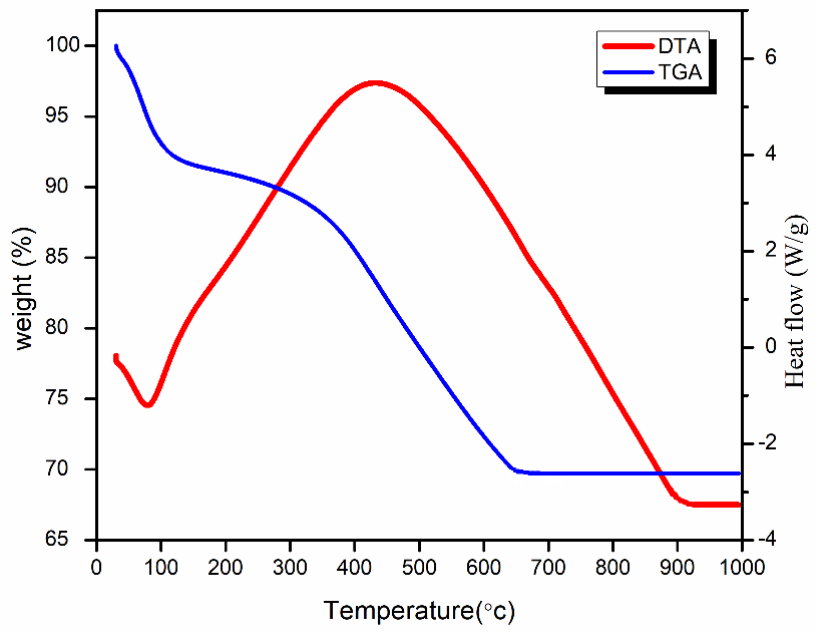


Figure 2. TGA-DTA analysis of raw CS.

Figure 3 shows the XRD pattern of CSHC. The pyrolyzed CSHC was investigated using X-ray diffraction (XRD), corroborating that the product is amorphous in nature and thus, it was precisely matched with the XRD pattern of hard carbon. Major changes in the peak position could not be observed. The broad peaks around 24° and 45° are due to (002) and (100), the diffraction planes. The characteristic peaks become broader and reduced intensity with activating agents (KOH, NaOH, $ZnCl_2$), insisting on the decrease in graphitic structure in CSHC [22]. These annotations revealed the degree of graphitization of the prepared HC sample was controlled by a chemical activating agent. These broad and low-intensity peaks designate the disordered nature of the CSHC samples [23]. The peak appears from the (002) of CSHC (K–CS, Na–CS, Zn–CS) corresponding to the interlayer distance of $d_{(002)}$ = 3.671, 3.704, and 3.943 Å due to varying the chemical activating agents. The interlayer spacing

and disordered structure of the synthesized materials further confirm that the CSHC is a suitable anode material for SIBs. Table 1 shows the structural properties of CSHC.

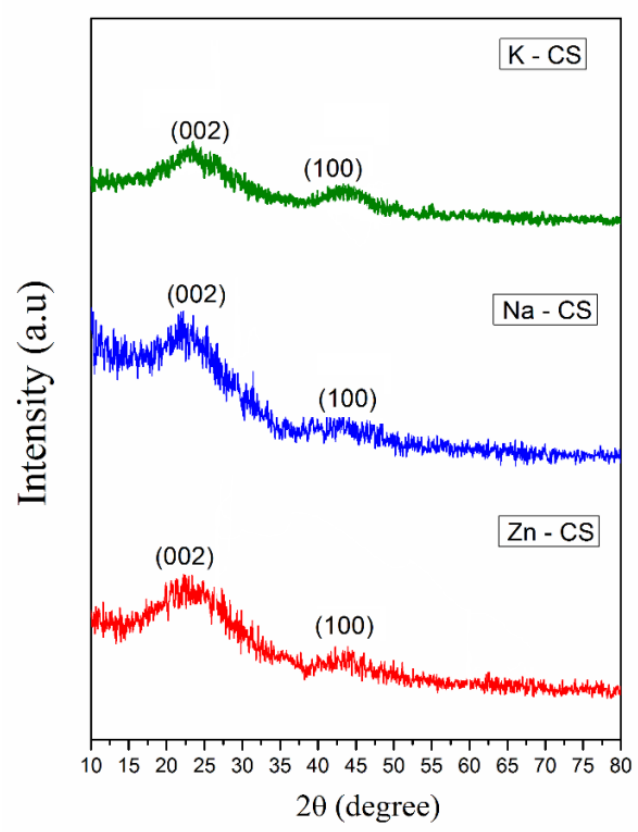


Figure 3. XRD analysis of K-CS, Na-CS, Zn-CS.

Table 1. Structural properties of CSHC.

Sl. No	Materials	d_{002} (Å)	$\frac{I_D}{I_G}$
1	K–CS	3.671	0.84
2	Na–CS	3.7049	0.85
3	Zn–CS	3.943	0.87

The occurrence of disordered hard carbon was further confirmed by Raman spectroscopy. Figure 4 shows the Raman spectra of K, Na, and Zn–CSHC. There are two distinct peaks around 1346 and 1582 cm^{-1}, assigned for the D–band and G–band of carbon. The D–band corresponds to the disordered while the G–band is the tangential vibrations of the carbon atom. The I_D/I_G (intensity ratios) of the synthesized K–CS, Na–CS, and Zn–CS are 0.84, 0.85, and 0.87. For all synthesis conditions, the I_D/I_G ratio never exceeds one, indicating that the materials are highly defective [16]. This result also confirms the occurrence of non-graphitizable HC with irregular structures. If the peak intensity of D band decreases, and the value of I_D/I_G increases continuously, indicating the ordered graphene sheets in the materials that are highly defective [24,25]. The increase of the I_D/I_G ratio for the KOH, NaOH, and $ZnCl_2$-treated HC suggests that harsh chemical treatments disturbed the structural order of the carbon. Hence, the synthesized HC indicates its appropriateness as an anode electrode material due to its outstanding electrical conductivity. This result agrees well with XRD data illustrations.

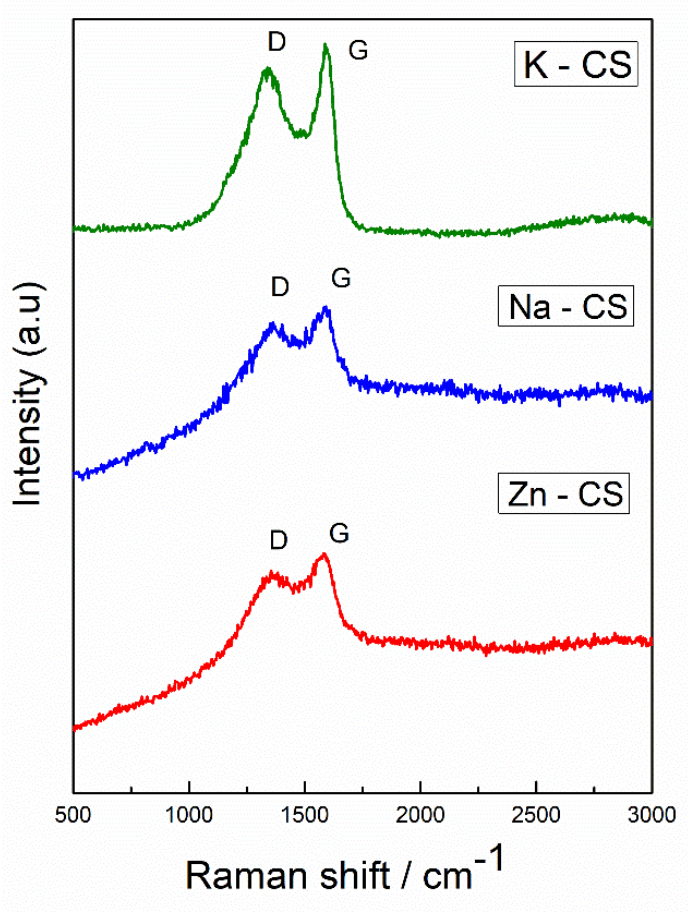


Figure 4. Raman spectrum of K-CS, Na-CS, Zn-CS.

FT-IR technique was used to determine the functional groups of the prepared (K–CS, Na–CS, Zn–CS) samples as shown in Figure 5. In the raw Coconut Sheath (CS) sample the bands at around 1206 cm^{-1} correspond to hemicellulose [26,27]. The bands at about 2942 cm^{-1} and 3413 cm^{-1} correspond to α–cellulose while the abiding bands fit into lignin. It can be evidently seen that the CSHC samples show noticeable characteristic bands of functional groups. The spectrum of carbon gave the absorption spectra of C=C at 1612 cm^{-1}, an intense band C–O at 1057 $cm^{-1,}$ and C–OH at 1376 cm^{-1} [28,29]. By comparing the raw CS and K–CS, Na–CS, and Zn–CS after carbonization, it is observed that the characteristic vibrational bands of those CH functional groups nearly vanish, and the IR curve is adjacent to a straight line with no obvious functional peaks, insisting that the CSHC is almost completely carbonized, in which the organic bonds are entirely decomposed to form hard carbon.

The scanning electron microscopy (SEM) was executed for all three CSHC precursors as shown in Figure 6. It is indisputable that the disordered, randomly oriented porous structure has been attained by KOH, NaOH, and $ZnCl_2$ activation. The SEM images exposed the effect of pyrolysis and chemical activation on the surface of carbon produced from the CS. The pyrolysis of the pre-carbonized precursor in the presence of KOH, NaOH, and $ZnCl_2$ creates open channels with little visible limited microporosity. Pinku Poddar et al. studied the mechanical, structural, and morphological study of coconut leaf sheath. In that study, they presented the SEM image of raw coconut leaf sheath precursor revealing a sheet-like structure, without any chemical activating agent. The raw CS turns into brown-colored powder after being dried and crushed. Subsequently, the powder turns black after chemical activation and pyrolysis. Here, all the HC particles show an irregular porous structure when compared to the above-mentioned untreated coconut leaf sheath, which means that the different chemical activating agents used have affected the size of the

particle and surface morphology of the HC material [30]. The existence of an open channel structure forms porous carbon, which allocates a path for the transportation of electrolyte ions during the charge storage process. The activation of carbon by KOH, NaOH, and $ZnCl_2$ proceeded according to the following reaction:

$$6KOH + C \rightarrow 2K + 3H_2 + 2K_2CO_3 \quad (1)$$

$$6NaOH + C \rightarrow 2Na + 3H_2 + 2\,Na_2CO_3 \quad (2)$$

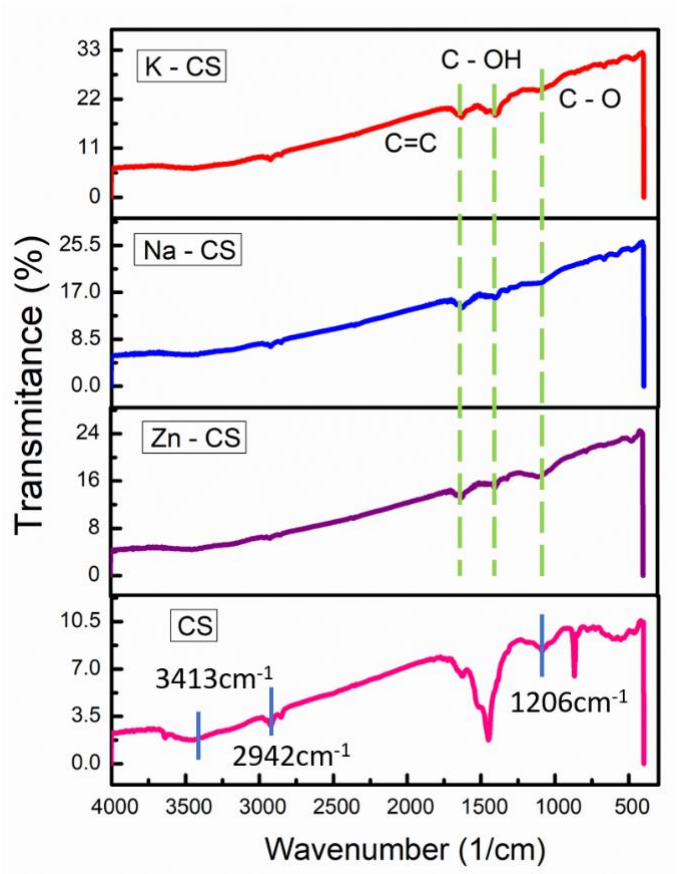


Figure 5. FTIR analysis of K-CS, Na-CS, Zn-CS.

The general stoichiometric reaction is given by:

$$6MOH + 2C \rightarrow 2M + 3H_2 + 2\,M_2CO_3 \quad (3)$$

The mechanism behind the chemical activation used is popular for several carbon materials. In KOH, the pore generation is primarily owing to the presence of oxygen in KOH, which results in the exclusion of stabilization and cross-linking of carbon atoms. At the pyrolysis temperature, the metallic K inserts into the carbon edifice and disrupts the arrangement of the crystallite. The porous nature is overseen by the amputation of potassium salts through washing and the removal of interior carbon atoms during the pyrolysis process [31,32].

In NaOH, the pore size is mainly due to some active sites in the char that are etched by strong corrosive NaOH at high temperatures. During the pyrolysis process, the ensuing char is richer in carbon, and the basic porous structure is formed by removing non-carbon atoms. In the interim, the char is rearranged for the crystal structure. This hampers the successive activation reactions with NaOH to generate a porous structure [33,34].

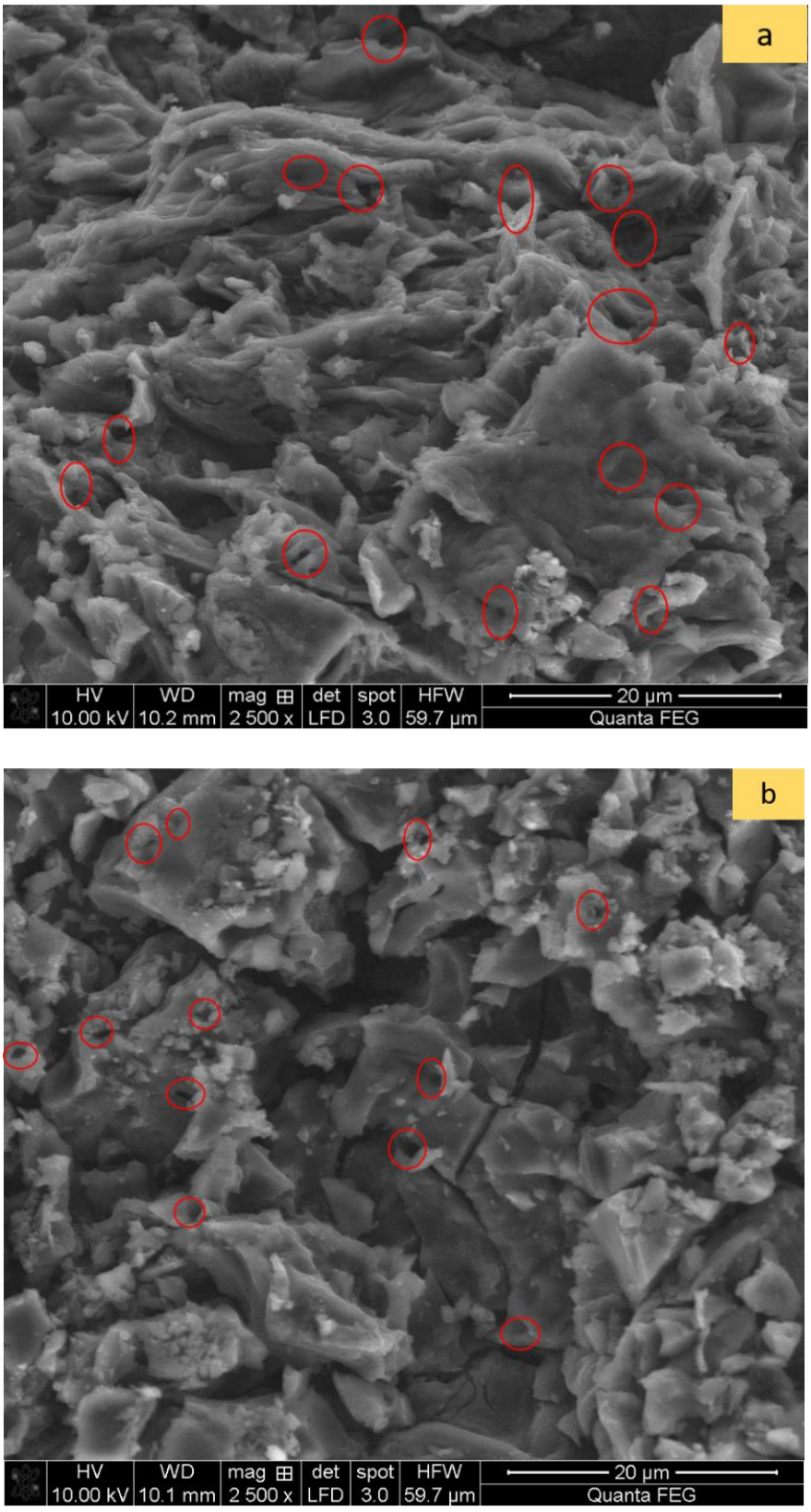


Figure 6. *Cont.*

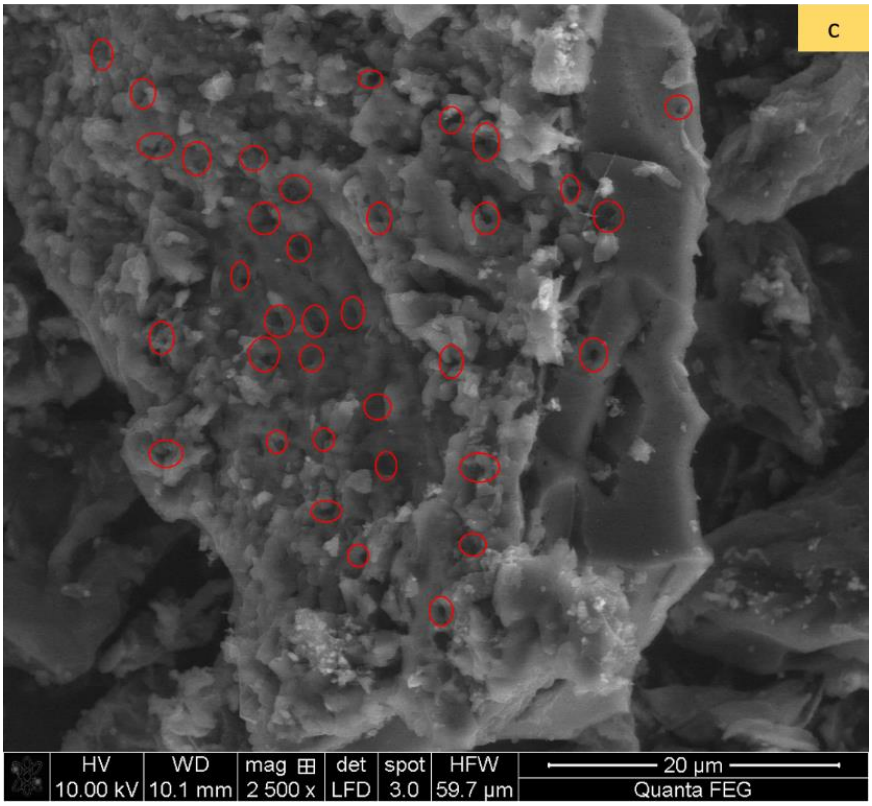


Figure 6. SEM analysis of (**a**) K-CS, (**b**) Na-CS, (**c**) Zn-CS.

In $ZnCl_2$, during pyrolysis, it acts as a dehydrating agent where aromatization and charring of carbon yield the formation of pores. After pyrolysis, in the washing stage, the unreacted $ZnCl_2$ salts can be removed, resulting in further pore generation [35]. In these three cases, there exists a mesoporous region. When compared to K–CS, Na–CS, and Zn–CS the Zn–CS has a more porous structure.

The TEM micrograph of the K–CS, Na–CS, and Zn–CS is shown in Figure 7. The irregular and randomly oriented structure observed indicates a disordered and amorphous HC. The material is categorized by the incidence of turbostratic graphitic domains scattered in a non–graphitic carbon matrix, as predicted for a distinctive hard carbon material. The interplanar separation (averaged) in the range of ~0.38 nm is detected by the TEM fringe analysis as can be evidently inferred from Figure 7. The specific separation in the carbon material compiles a synthesized HC as an appropriate choice for reversible intercalation/deintercalation of Na ions.

The nitrogen adsorption and desorption were analyzed for K–CS, Na–CS, and Zn–CS samples. Table 2 Describes the textural data of the synthesized samples. Figures 8 and 9 show the specific surface area and pore size of the synthesized carbon materials which were influenced by the activating agents (KOH, NaOH, $ZnCl_2$). It can be discovered that a typical IV isotherm with a well-defined hysteresis pressure P/P_0 of K–CS, Na–CS, Zn–CS samples between 0.3 and 0.95, the isotherms display a sharp step characteristic of capillary condensation of nitrogen within uniform mesopores, where the P/P_0 position of the inflection point is correlated to the diameter of the mesopore [36,37]. It also specifies the occurrence of some open mesopores. Though, the hysteresis loop progressively shrinks with the increase in hard carbon loading, signifying that there is a clear change in the nanopores of the materials after the activation process. Particularly for the samples Zn–CS, the hysteresis loop fades, and the total nitrogen adsorption volume reduces to the minimum. The specific surface areas of K–CS, Na–CS, and Zn–CS are calculated to be 153.3 m^2/g, 79.240 m^2/g, and 20.780 m^2/g, and are shown in Table 2. The surface area also plays an imperative role in improving the EC performance of CSHC. Combined with SEM results,

Figure 6 shows the partial decrease in surface area (S_{BET}), which is likely produced by the thermal deposition of the volatiles into the defective nanopores, which acts as a pore healing process during carbonization [38].

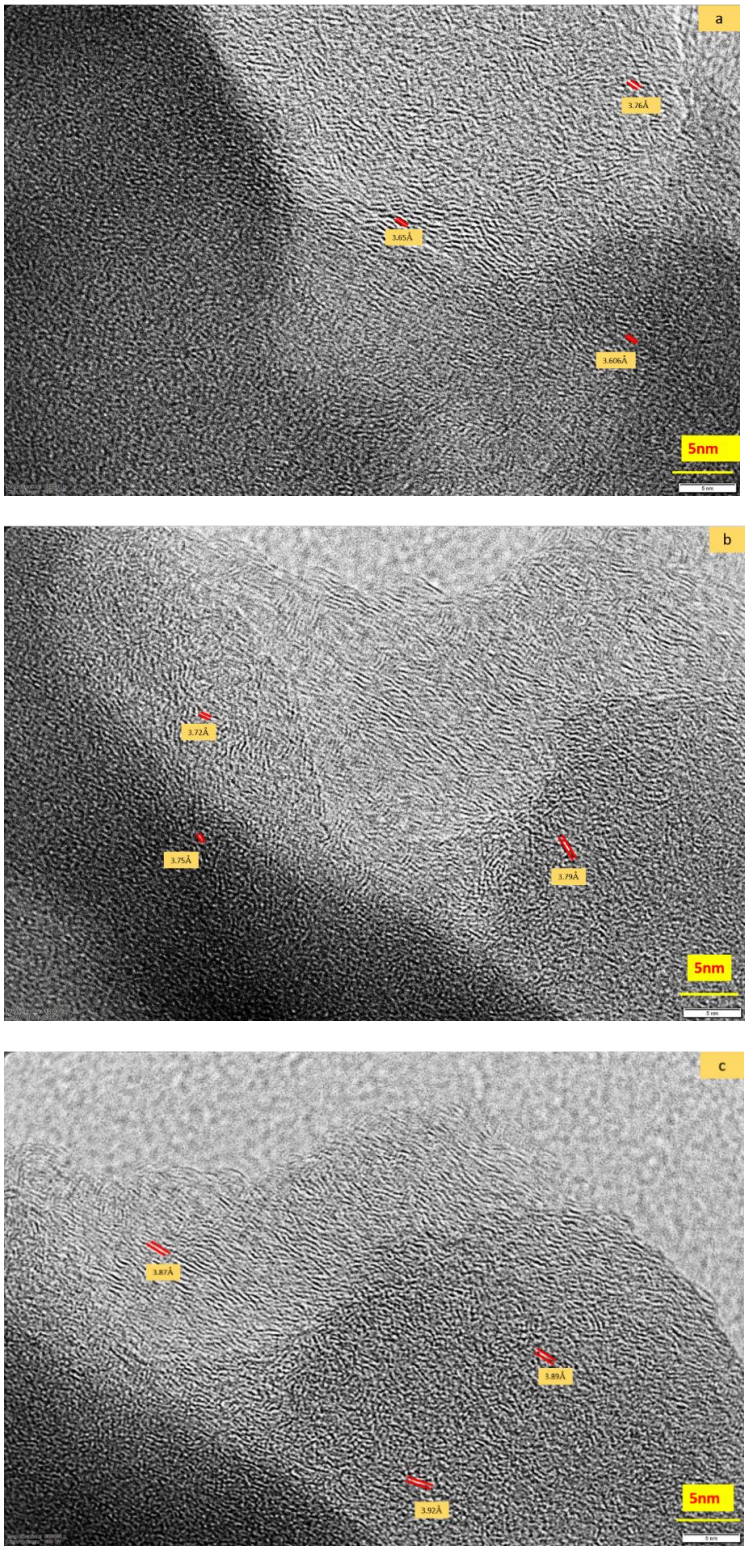


Figure 7. TEM analysis of (**a**) K-CS, (**b**) Na-CS, (**c**) Zn-CS.

Table 2. Textural properties of CSHC.

S.No	Sample	Surface Area (m^2/g)	Pore Diameter (nm)	Pore Volume (cc/g)
1.	K–CS	153.3	3.059	0.004
2.	Na–CS	79.240	3.757	0.031
3.	Zn–CS	20.780	3.772	0.158

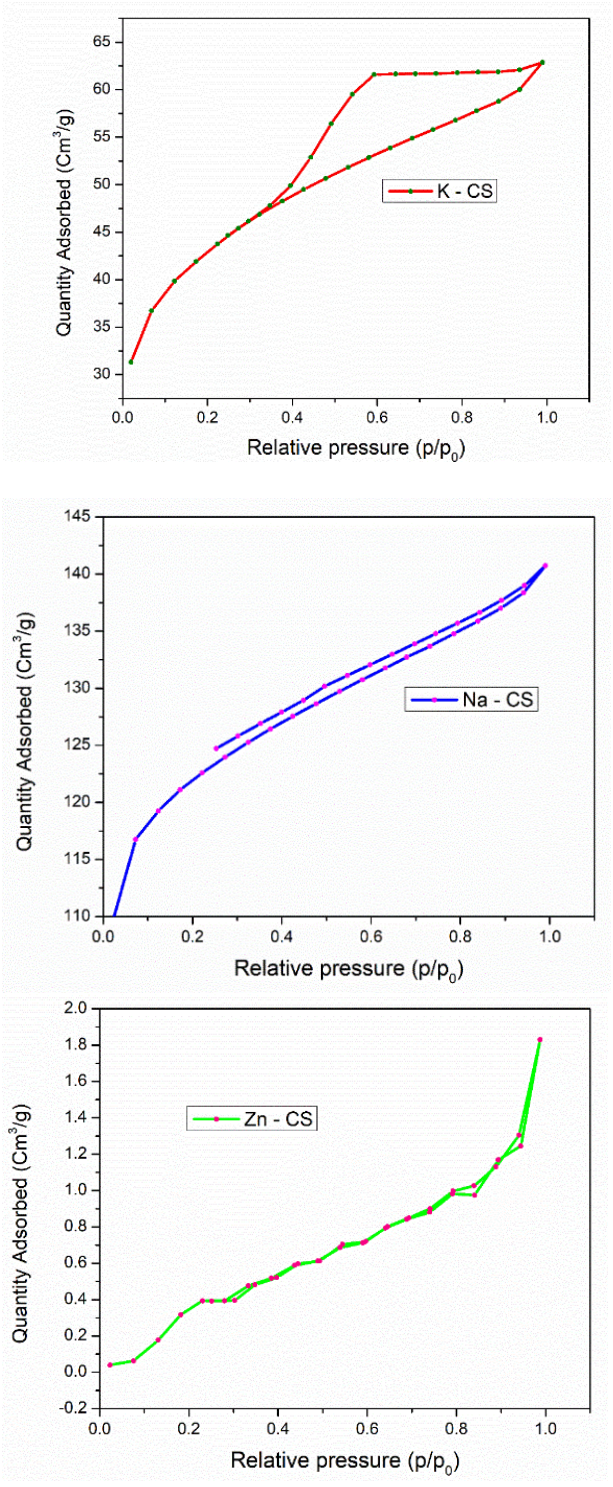


Figure 8. N_2 adsorption and desorption analysis of K-CS, Na-CS, Zn-CS.

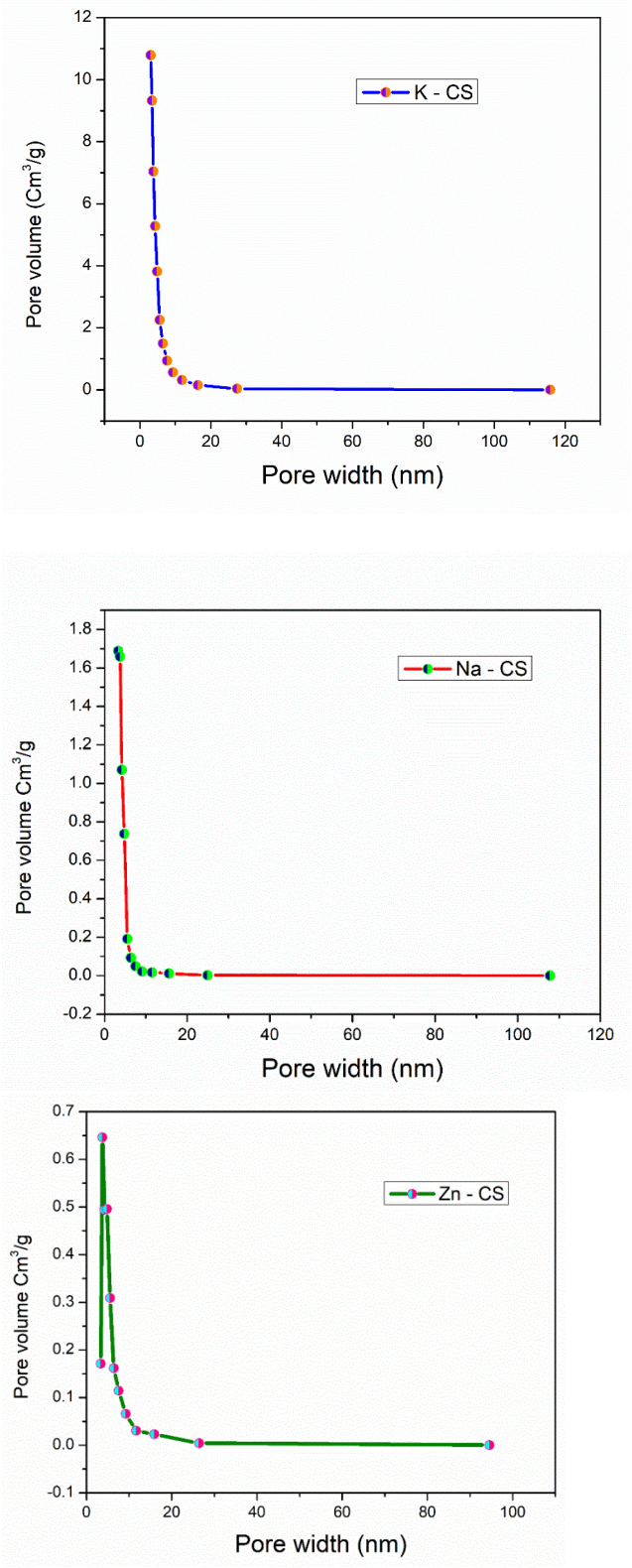


Figure 9. Pore size distribution of K-CS, Na-CS, Zn-CS.

The pore diameter of the carbon materials has shown a significant increase after the treatment of activating agents. The pore diameter of K–CS, Na–CS, and Zn–CS is 3.059 nm, 3.757, and 3.772 nm, respectively. The prepared mesopore carbon materials having a smaller specific area leads to high coulombic efficiency in battery applications. It can be assessed that while the pore diameter elevates the surface area can be demoted, i.e., pore diameter

and surface area are contrarily proportional [16]. Ideally, the material is contemplated for SIBs only when the surface area is very low. This is primarily because of the creation of a solid electrolyte interface (SEI) and electrolyte deprivation. From this perspective, CSHC can be used for SIBs.

To explicate the electrochemical nature of K–CS, Na–CS, Zn–CS, the cyclic voltammetry tests in half calls for the first three cycles have been performed with Na as a counter electrode between 0.01 and 3 V with a scanning rate of 0.1 mVS^{-1}.

The CV curve of the as-prepared material was shown in Figure 10. It demonstrates that there are no sharp peaks can be observed during scanning. These sharp peaks are accredited to the formation of the electrolyte interface. The lesser surface area of the material may persuade the limited formation of SEI, and hence it could improve the initial coulombic efficiency of K–CS, Na–CS, and Zn–CS at 99.5%, 99.3%, and 98.8%. These high initial coulombic efficiencies can be obtained due to less oxygenated groups which are confirmed in FT-IR analysis and have smaller specific surface area. In addition to that, the functional groups present in the carbon also seem to be another appropriate parameter that affects the capacity of the material. In this context, the as-fabricated HC materials (K–CS, Na–CS, Zn–CS) demonstrate good cycling stability, especially in the cycling process, Zn–CS has less capacity fading when compared to Na–CS and K–CS. The first three curves of K–CS, Na–CS, Zn–CS implies that the as-prepared HC materials have stable cycle performance in long term cycling tests.

The galvanostatic charge/discharge profile of K–CS, Na–CS, and Zn–CS anode material was performed between 0.01 and 2.8 V at 1 C, and it was revealed in Figure 11. Tao Zhang et al. and Linyuan Pei et al. stated that the hard carbon anode material yields an initial charge capacity of 86 mAh g^{-1} and 88 mAh g^{-1}, respectively. Moreover, Huimin Zhang et al. analyzed that the HC electrode material delivers a reversible charge capacity of 95 mAh g^{-1} as shown in Table 3. In this work, the CSHC anode material delivers an initial charge capacity of 162, 153, and 141 mAh g^{-1}, which is significantly higher than the preceding reports. Therefore, the chemical activating agent theaters a substantial role in improving the electrochemical performance of HC anode material while employed in SIBs. The NaOH, KOH, and $ZnCl_2$ corrode the carbon matrix and improve the porous nature of the material which is more responsible for enhancing the structural stability during the charging/discharging process [39,40]. The working mechanism of activating agents is explained briefly in the above SEM analysis. Furthermore, the as-prepared anode materials deliver the reversible charge capacity of 141–72 mAh g^{-1}, for K-CS, 153–80 mAh g^{-1} for Na–CS, and 162–117 mAh g^{-1} for Zn–CS in the cycles ranging from 2 to 100, respectively. The K–CS, Na–CS, and Zn–CS releases a reversible capacity of 141, 153, and 162 mAh g^{-1} in the initial cycle and maintains 72, 80, 117 mAh g^{-1} with 51.1%, 52.05%, and 72% of capacity retention and 98.8%, 99.3%, and 99.5% of coulombic efficiency after 100th cycle was shown in Figure 12, which proposes the worthy electrochemical performance. The rate capability of K–CS, Na–CS, and Zn–CS anode material was analyzed at diverse current rates from 1C to 5C and it is shown in Figure 13. For 1 C, 2C, 3C, and 5C the K–CS delivers the charge capacity of 141, 126, 100, and 61. The Na–CS delivers the charge capacity of 153, 131, 96, and 71. The Zn–CS anode material delivers the charge capacity of 162, 154, 124, and 97, respectively. When the current density was returned to a lower rate, i.e., 1C, the original capacity was almost recovered (137, 149, and 161 mAh g^{-1}); it demonstrates the good electrochemical performance of K–CS, Na–CS, and Zn–CS. When comparing these three-anode materials the Zn–CS shows a high reversible charge capacity of 162 and higher capacity retention of 72% when compared to Na–CS and K–CS.

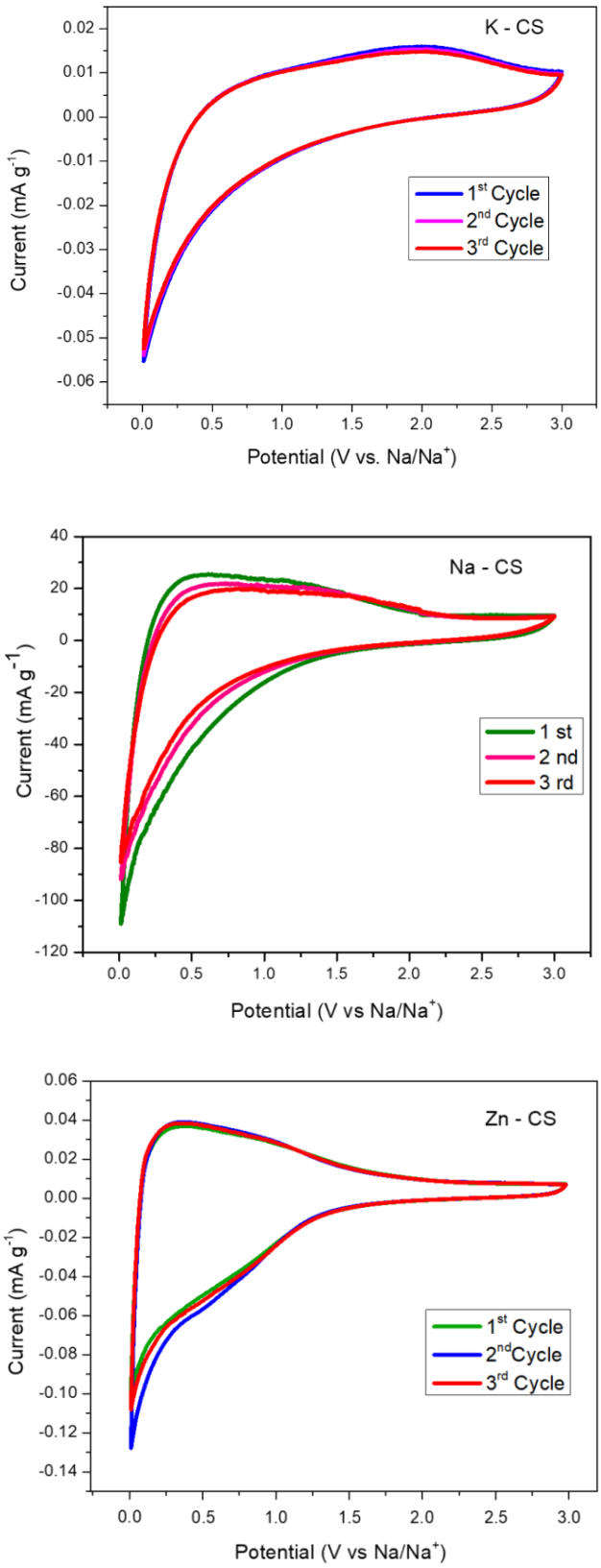


Figure 10. Cyclic voltammetry curve of K-CS, Na-CS, Zn-CS.

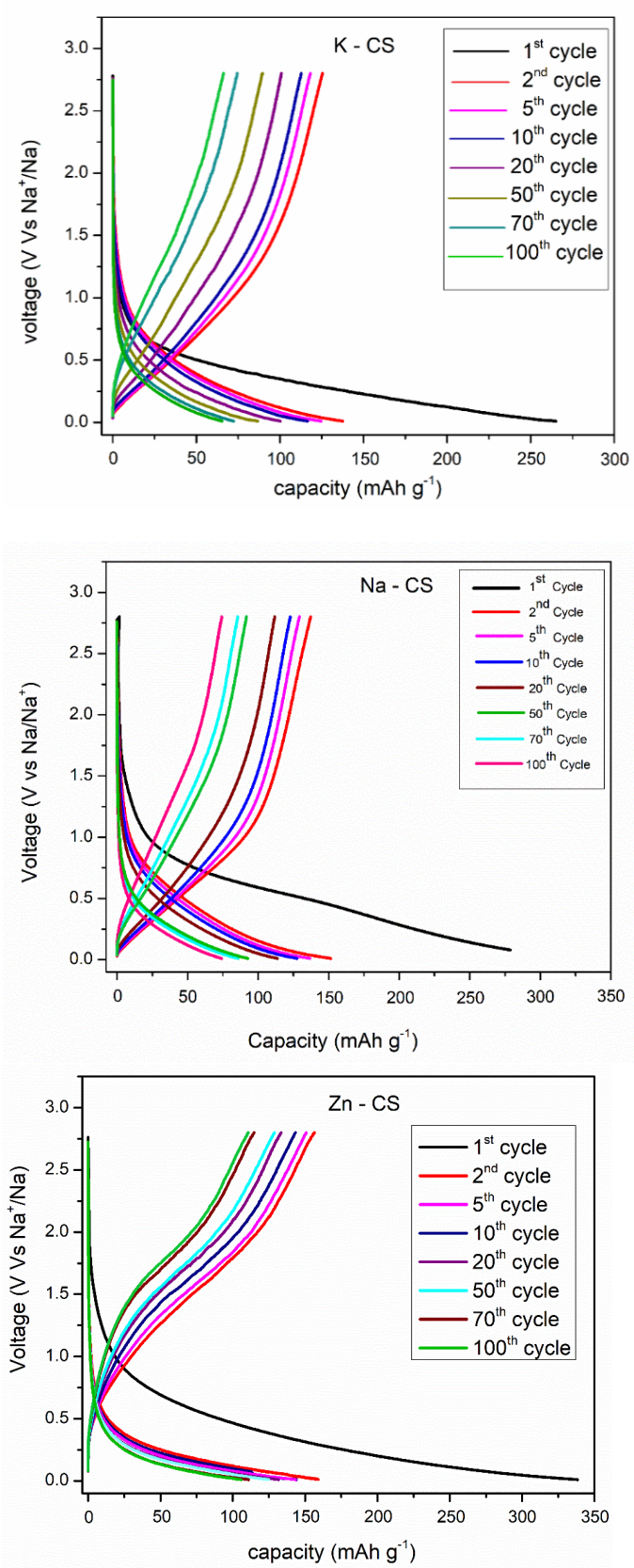


Figure 11. Galvanostatic charge/discharge performance of K-CS, Na-CS, Zn-CS.

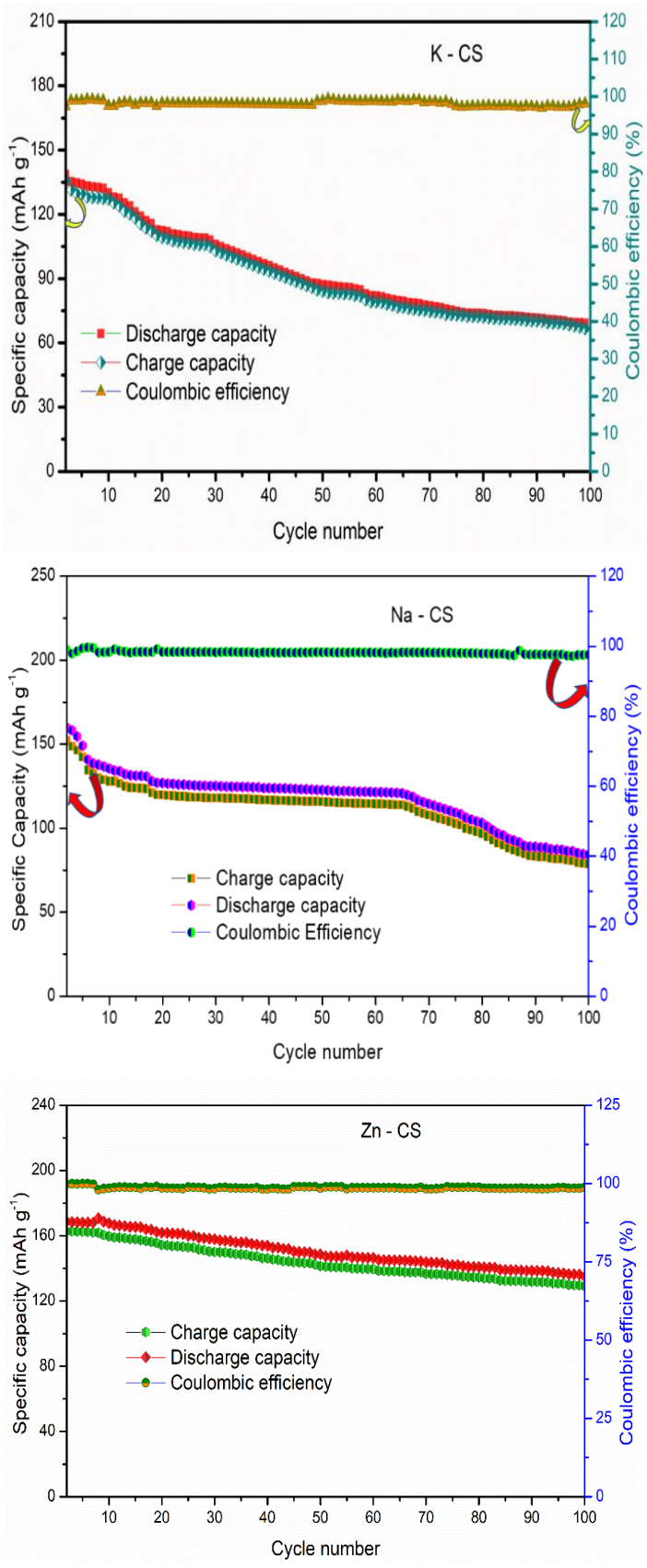


Figure 12. Cyclic performance and efficiency of K-CS, Na-CS, Zn-CS.

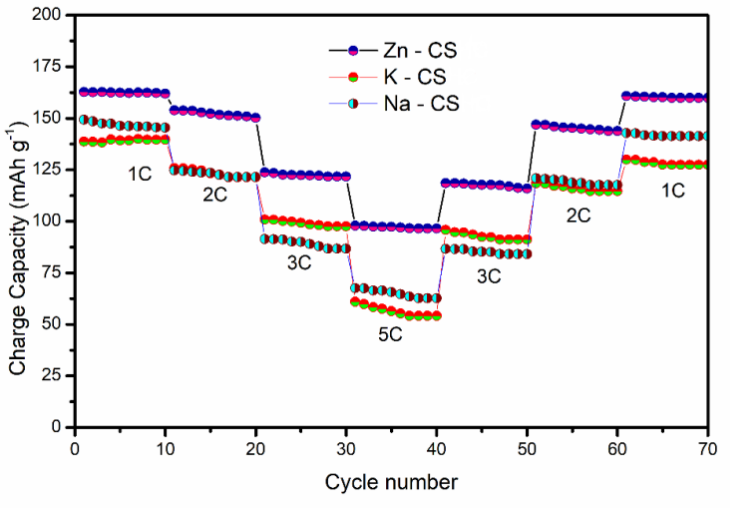


Figure 13. Rate capability of K-CS, Na-CS, Zn-CS.

Table 3. Comparison of different hard carbon materials as anodes for SIBs.

Anode Materials	Capacity (mAh g^{-1})	Current Density (mAg^{-1})	Reference
Hard Carbon from corn straw piths (HC 1400, HC 1600)	120 mAh g^{-1}, 80 mAh g^{-1}	1C	[40]
Hard Carbon from sucrose/PF precursors (HCM 1000, HCM 1200, HCM 1600)	95 mAh g^{-1}, 105 mAh g^{-1}, 68 mAh g^{-1}	1C	[38]
Hard Carbon from waste tea biomass (PWT 1200, PWT 1400, PWT 1600)	88 mAh g^{-1}, 95 mAh g^{-1}, 70 mAh g^{-1}	1C	[37]
Pinecone bio-mass derived Hard Carbon (PHC 1000, PHC 1200, PHC 1600)	86 mAh g^{-1}, 99 mAh g^{-1}, 43 mAh g^{-1}	1C	[36]
Coconut Sheath Derived Hard Carbon (K-CS, Na-CS, Zn-CS)	141.27 mAh g^{-1}, 153.02 mAh g^{-1}, 162.30 mAh g^{-1}	1C	Present work

Electrochemical impedance spectra (EIS) were analyzed with an AC amplitude of 10 mV using a biologic (BCS-815, France) battery tester, with a frequency from 10 kHz to 1 Hz at room temperature. The enhancement of the material's conductivity is confirmed by electrochemical impedance spectroscopy (EIS). The EIS Nyquist plot equivalent circuit (inset) of K–CS, Na–CS, and Zn–CS anode material is presented in Figure 14. The Nyquist plot comprises a semicircle (high-frequency region) and an inclined line (low-frequency region). In the equivalent circuit R_{CT}, represents charge transfer resistance at the electrolyte/electrode interface, R_S designates the solution resistance or ohmic resistance which is the total resistance of the cell. CPE denotes the constant phase element and Z_W corresponds to the Warburg resistance that implies the Warburg diffusion in the cell. The value of R_{CT} for the K–CS, Na–CS, and Zn–CS cells are 139, 118, and 129 Ω, and R_s value for the K–CS, Na–CS, and Zn–CS cells are 87, 56, and 26 Ω respectively, which signifies that the sodium ions migrate easily during the cycling process. The frequency from high to medium semicircle could be evinced for the K–CS, Na–CS, and Zn–CS materials for their low charge transfer resistance, which leads to the noticeable electrochemical performance of CSHC. When compared to these materials (K–CS, Na–CS, Zn–CS) the Zn–CS has low R_s value. Hence, it has the best electrochemical performance for SIBs.

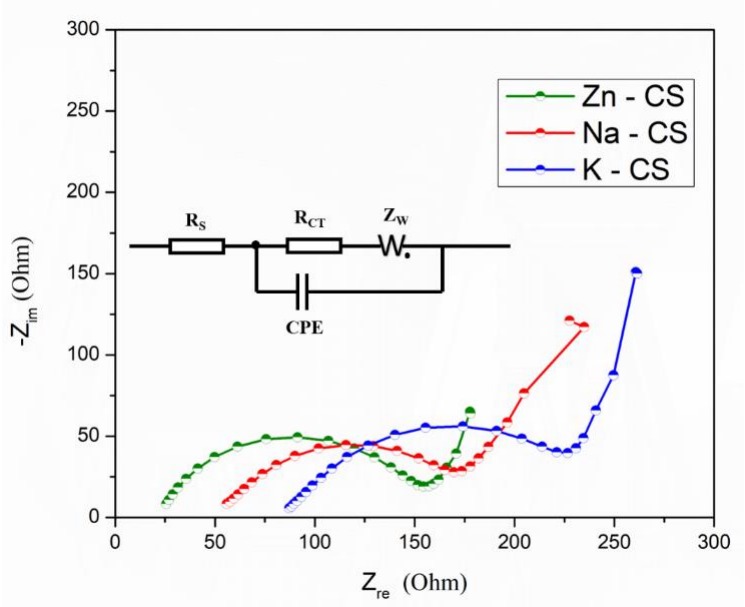


Figure 14. Nyquist plot of K-CS, Na-CS, Zn-CS.

4. Conclusions

In this exertion, the CSHC has been successfully synthesized by a simple pyrolysis method and made a porous structure using various activating agents (KOH, NaOH, and $ZnCl_2$). The CSHC anode exhibit better electrochemical performance that can meet the necessities of large-scale commercial applications. The above-obtained results confirm the high initial coulombic efficiency and durability behavior of the HC material. The CSHC anode discloses the initial charge capacity of 141 mAh g^{-1}, 153 mAh g^{-1}, and 162 mAh g^{-1} at a 1 C rate. The material has low surface areas (153.3 m^2/g, 79.240 m^2/g, 20.78 m^2/g) with a high initial coulombic efficiency of 98.8%, 99.3%, and 99.5%, even after 100 cycles. These tremendous properties suggests that CSHC is one of the most proficient anode materials for large-scale SIBs applications.

Author Contributions: Conceptualization, M.T., S.R., and S.M.; data curation, M.T., S.R., and S.M.; formal analysis, M.T., S.R., and S.M.; funding acquisition, S.R. and S.M.; investigation, M.T., S.R., and S.M.; methodology, M.T., S.R., and S.M.; project administration, S.R. and S.M.; resources, S.R. and S.M.; software, S.R. and S.M.; supervision, S.R. and S.M.; validation, M.T., S.R., and S.M.; visualization, S.R. and S.M.; writing—original draft, M.T., S.R., and S.M.; writing—review and editing, M.T., S.R., and S.M. All authors have read and agreed to the published version of the manuscript.

Funding: All the authors from Alagappa University acknowledge the financial support by DST SERB, New Delhi, India under the Physical sciences, grant sanctioned vide EMR/2016/006302 and Ministry of Human Resource Development RUSA- Phase 2.0 grant sanctioned vide Lt.No.F-24-51/2014 U Policy (TNMulti Gen), Dept. of Education, Govt. of India.

Data Availability Statement: Not Applicable.

Conflicts of Interest: All the authors declare that there is no conflict of interest.

References

1. Xiao, B.; Rojo, T.; Li, X. Hard carbon as sodium-ion battery anodes: Progress and challenges. *Chem. Sus. Chem.* **2019**, *12*, 133–144. [CrossRef] [PubMed]
2. Malik, A.W. *Targeted Synthesis of Functional Soft and Hard Carbons from Bio-Waste and Natural Products for Supercapacitor and Battery Applications*; CSIR-National Chemical Laboratory: Pune, India, 2016.
3. Thomson, M.; Xia, Q.; Hu, Z.; Zhao, X.S. A review on biomass–derived hard carbon materials for sodium-ion batteries. *Mater. Adv.* **2021**, *2*, 5881–5905. [CrossRef]
4. Lach, J.; Wrobel, K.; Wrobel, J.; Czerwinski, A. Applications of carbon in rechargeable electrochemical power sources: A review. *Energies* **2021**, *14*, 2649. [CrossRef]

5. Qu, D. Fundamental principles of battery design: Porous electrodes. In *AIP Conference Proceedings*; American Institute of Physics, AIP publishing: New York, NY, USA, 2014; Volume 1597, pp. 14–25.
6. Ranaweera, C.K.; Kahol, P.K.; Ghimire, M.; Mishra, S.R.; Gupta, R.K. Orange-peel-derived carbon: Designing sustainable and high-performance supercapacitor electrodes. *C* **2017**, *3*, 25. [CrossRef]
7. Ding, J.; Wang, H.; Li, Z.; Kohandehghan, A.; Cui, K.; Tan, X.; Lotfabad, E.M.; Olsen, B.C. Carbon Nanosheet Frameworks Derived from Peat Moss as High-Performance Sodium Ion Battery Anodes. *ACS Nano* **2013**, *7*, 11004–11015. [CrossRef] [PubMed]
8. Memarzadeh Lotfabad, E.; Ding, J.; Cui, K.; Kohandehghan, A.; Kalisvaart, W.P.; Hazelton, M.; Mitlin, D.; Lotfabad, E.M.; Ding, J.; Cui, K. High-Density Sodium and Lithium-Ion Battery Anodes from Banana Peels. *ACS Nano* **2014**, *8*, 7115–7129. [CrossRef]
9. Wang, P.; Qiao, B.; Du, Y.; Li, Y.; Zhou, X.; Dai, Z.; Bao, J. Fluorine-Doped Carbon Particles Derived from Lotus Petioles as High-Performance Anode Materials for Sodium-Ion Batteries. *J. Phys. Chem. C* **2015**, *119*, 21336–21344. [CrossRef]
10. Zhao, H.; Gao, Y.; Wang, J.; Chen, C.; Chen, D.; Wang, C.; Ciucci, F. Egg Yolk-Derived Phosphorus and Nitrogen Dual Doped Nano Carbon Capsules for High-Performance Lithium-Ion Batteries. *Mater. Lett.* **2016**, *167*, 93–97. [CrossRef]
11. Cao, X.; Chen, S.; Wang, G. Porous Carbon Particles Derived from Natural Peanut Shells as Lithium-Ion Battery Anode and Its Electrochemical Properties. *Electron. Mater. Lett.* **2014**, *10*, 819–826. [CrossRef]
12. Shen, F.; Luo, W.; Dai, J.; Yao, Y.; Zhu, M.; Hitz, E.; Li, X. Ultra-Thick, Low-Tortuosity, and Mesoporous Wood Carbon Anode for High-Performance Sodium-Ion Batteries. *Adv. Energy Mater.* **2016**, *6*, 1600377. [CrossRef]
13. Lv, W.; Wen, F.; Xiang, J.; Zhao, J.; Li, L.; Wang, L.; Liu, Z.; Tian, Y. Peanut Shell Derived Hard Carbon as Ultralong Cycling Anodes for Lithium and Sodium Batteries. *Electrochim. Acta* **2015**, *176*, 533–541. [CrossRef]
14. Shen, F.; Zhu, H.; Luo, W.; Wan, J.; Zhou, L.; Dai, J.; Zhao, B.; Han, X.; Fu, K.; Hu, L. Chemically Crushed Wood Cellulose Fiber towards High-Performance Sodium-Ion Batteries. *ACS Appl. Mater. Interfaces* **2015**, *7*, 23291–23296. [CrossRef] [PubMed]
15. Yang, T.; Qian, T.; Wang, M.; Shen, X.; Xu, N.; Sun, Z.; Yan, C.A. Sustainable Route from Biomass Byproduct Okara to High Content Nitrogen-Doped Carbon Sheets for Efficient Sodium Ion Batteries. *Adv. Mater.* **2016**, *28*, 539–545. [CrossRef] [PubMed]
16. Meenatchi, T.; Priyanka, V.; Subadevi, R.; Liu, W.R.; Huang, C.H.; Sivakumar, M. Probe on hard carbon electrode derived from orange peel for energy storage application. *Carbon Lett.* **2021**, *31*, 1033–1039. [CrossRef]
17. Gunn, B.F.; Baudouin, L.; Olsen, K.M. Independent origins of cultivated Coconut (*Cocos nucifera* L.) in the old world tropics. *PLoS ONE* **2011**, *6*, e21143. [CrossRef]
18. Jose, N. Coconut Leaf—Sheath Scales as an Effective Medicine for Wound Healing. 2006. Available online: https://www.researchgate.net/publication/260208418_Coconut_Leaf-sheath_Scales_as_an_Effective_Medicine_for_Wound_Healing (accessed on 8 October 2022).
19. Khornia, D.L.L.F.; Rita, D.R.; Nurk, S. Analysis comparison npp thorium fuel as an alternative energy sources. *Inovari Tek. Kim.* **2017**, *11*, 32–38.
20. Muruganantham, R.; Sivakumar, M.; Subadevi, R.; Wu, N.L. A facile synthesis and characterization of $LiFePO_4$/C using simple binary reactants with oxalic acid by polyol technique and other high-temperature methods. *J. Mater. Sci. Mater. Electron.* **2015**, *26*, 2095–2106. [CrossRef]
21. Srinivasan, V.S.; Boopathy, S.R.; Sangeetha, D.; Ramnath, B.V. Evaluation of mechanical and thermal properties of banana–flax based natural fibre composite. *Mater. Des.* **2014**, *60*, 620–627. [CrossRef]
22. Short, M.A.; Walker, J.P.L. Measurement of interlayer spacings and crystal sizes in turbostratic carbons. *Carbon* **1963**, *1*, 3–9. [CrossRef]
23. Wang, K.; Jin, Y.; Sun, S.; Huang, Y.; Peng, J.; Luo, J.; Zhang, Q.; Qiu, Y.; Fang, C.; Han, J. Low-cost and High-performance hard carbon anode materials for sodium-ion batteries. *ACS Omega* **2017**, *2*, 1687–1695. [CrossRef]
24. Krishnaveni, K.; Subadevi, R.; Raja, M.; Premkumar, T.; Sivakumar, M. Sulfur/PAN/acetylene black composite prepared by a solution processing technique for lithium-sulfur batteries. *J. Appl. Polym. Sci.* **2018**, *135*, 46598.
25. Poddar, P.; Asad, M.A.; Islam, M.S.; Sultana, S.; Nur, H.P.; Chowdhury, A.S. Mechanical and morphological study of arecanut leaf sheath (ALS), coconut leaf sheath (CLS) and coconut stem fiber (CSF). *Adv. Mater. Sci.* **2016**, *1*, 1–4. [CrossRef]
26. Pandey, K.K. A study of chemical structure of soft and hardwood and wood polymers by FTIR spectroscopy. *J. Appl. Polym. Sci.* **1999**, *71*, 1969–1975. [CrossRef]
27. Rao, X.; Lou, Y.; Chen, J.; Lu, H.; Cheng, B.; Wang, W.; Fang, H.; Li, H.; Zhong, S. Polyacrylonitrile hard carbon as anode for high-rate capability for lithium-ion batteries. *Front. Energy Res.* **2020**, *8*, 3. [CrossRef]
28. Rochman, R.A.; Wahyuningsih, S.; Ramelan, A.H.; Hanif, Q.A. Preparation of nitrogen and sulphur Co-doped reduced graphene oxide (rGO-NS) using N and S heteroatom of thiourea. *IOP Conf. Ser. Mater. Sci. Eng.* **2019**, *509*, 012119. [CrossRef]
29. Satyanarayana, K.; Pillai, C.K.S.; Sukumaran, K.; Pillai, S.G.K. Structure property studies of fibres from various parts of the coconut tree. *J. Mater. Sci.* **1982**, *17*, 2453–2462. [CrossRef]
30. Lillo-Rodenas, M.A.; Cazorla-Amoros, D.; Linares-Solano, A. Understanding chemical reactions between carbons and NaOH and KOH: An insight into the chemical activation mechanism. *Carbon* **2003**, *41*, 267–275. [CrossRef]
31. Lillo-Rodenas, M.A.; Juan-Juan, J.; Cazorla-Amoros, D.; Linares-Solano, A. About reactions occurring during chemical activation with hydroxides. *Carbon* **2004**, *42*, 1371–1375. [CrossRef]
32. Xu, B.; Chen, Y.; Wei, G.; Cao, G.; Zhang, H.; Yang, Y. Activated carbon with high capacitance prepared by NaOH activation for supercapacitors. *Mater. Chem. Phys.* **2010**, *124*, 504–509. [CrossRef]

33. Subramanian, V.; Luo, C.; Stephan, A.M.; Nahm, K.S.; Thomas, S.; Wei, B. Supercapacitors from activated carbon derived from banana fibers. *J. Phys. Chem. C* **2007**, *111*, 7527–7531. [CrossRef]
34. Ulfa, M.; Trisunaryanti, W.; Falah, I.I.; Kartini, I.; Sutarno, I. Synthesis of meso porous carbon using gelatin as source of carbon by hard template technique and its characterizations. *IOSR J. Appl. Chem.* **2014**, *7*, 1–7. [CrossRef]
35. Ge, C.; Fan, Z.; Zhang, J.; Qiao, Y.; Wang, J.; Ling, L. Novel hard carbon/graphite composites synthesized by a facile in situ anchoring method as high-performance anodes for lithium-ion batteries. *RSC Adv.* **2018**, *8*, 34682–34689. [CrossRef] [PubMed]
36. Zhang, T.; Mao, J.; Liu, X.; Xuan, M.; Bi, K.; Zhang, X.L.; Hu, J.; Fan, J.; Chen, S.; Shao, G. Pinecone biomass-derived hard carbon anodes for high-performance sodium-ion batteries. *RSC Adv.* **2017**, *7*, 41504–41511. [CrossRef]
37. Pei, L.; Cao, H.; Yang, L.; Liu, P.; Zhao, M.; Xu, B.; Guo, J. Hard carbon derived from waste tea biomass as high-performance anode material for sodium-ion batteries. *Ionics* **2020**, *26*, 5535–5542. [CrossRef]
38. Zhang, H.; Ming, H.; Zhang, W.; Cao, G.; Yang, Y. Coupled carbonization strategy toward advanced hard carbon for high-energy sodium-ion battery. *ACS Appl. Mater. Interfaces* **2017**, *9*, 23766–23774. [CrossRef] [PubMed]
39. Wahid, M.; Gawli, Y.; Puthusseri, D.; Kumar, A.; Shelke, M.V.; Ogale, S. Nutty carbon: Morphology replicating hard carbon from walnut shell for Na ion battery anode. *ACS Omega* **2017**, *2*, 3601–3609. [CrossRef] [PubMed]
40. Zhu, Y.E.; Gu, H.; Chen, Y.N.; Yang, D.; Wei, J.; Zhou, Z. Hard carbon derived from corn straw piths as anode materials for sodium ion batteries. *Ionics* **2018**, *24*, 1075–1081. [CrossRef]